

# Quantum States and Atomic Structure of Silicon Surfaces

R. M. TROMP, R. J. HAMERS, J. E. DEMUTH

The electronic and geometric structures of surfaces are closely related to each other. Conventional surface science techniques can study one or the other, but not both at the same time. Recent developments in scanning tunneling microscopy have made it possible to study simultaneously the electronic and geometric structure of Si(111) and Si(001) surfaces. Surface states can be atomically resolved in space and energy; thus the electronic structure of single atoms on surfaces can be studied in detail. The various surface states observed on silicon surfaces are found to derive from different atomic-scale features in the surface geometric structure. Scanning tunneling microscopy has now bridged the gap between electronic and geometric structure, providing a unique opportunity to obtain a better understanding of many surface processes at the atomic level.

SILICON SURFACES ARE WELL KNOWN FOR THEIR TENDENCY to reconstruct. The size of the crystallographic unit cell at the surface is larger than in the bulk because the surface atoms rearrange themselves in a geometric structure that may be different from that of the underlying bulk lattice. This phenomenon of surface reconstruction is a consequence of the fact that in a bulklike terminated surface the atoms are not fourfold coordinated because some of their neighbors are missing. The broken bonds give rise to a high surface energy that drives the surface atoms to rearrange themselves. The surface energy may be lowered by decreasing the number of broken bonds, increasing the bond strength in the surface, or both. These unusual surface bonds also give rise to localized electronic quantum states that do not exist in the bulk of the crystal. It is the interplay between these quantum states and the surface geometry that eventually determines which structure is assumed.

## Electron States and Surface Geometry

Traditionally, surface geometry and surface electronic structure have been studied by different experimental probes. Most techniques that are sensitive to geometric structure cannot address the electronic structure (electron diffraction, ion scattering, atom scattering, and the like), whereas techniques that are well suited for studying surface electron states have no direct access to the geometric structure (for instance, photoemission spectroscopy, electron energy loss spectroscopy, and bremsstrahlung spectroscopy) (1). This gap between geometric and electronic probes has now been bridged by a technique invented 3 years ago by Binnig and

colleagues (2) of the IBM Research Laboratory in Zürich, Switzerland. With this technique, called scanning tunneling microscopy (STM), the IBM researchers were able to obtain the first atomically resolved real-space images of the structure of the famous Si(111)-(7×7) surface (3), in which the unit cell is seven times larger than the bulk unit cell along both independent surface lattice directions.

STM is not only sensitive to the surface geometry but also to the surface electronic structure. STM images in general contain a mixture of both contributions, and efforts to separate these on an atomic scale have been limited. Previous bias-dependent measurements attempting to obtain spectroscopic information were incomplete because data could only be obtained over a limited spectroscopic range or at only a few positions on the surface (4). In one case, a defect state lying in an energy band gap was imaged (5). In this article we describe recent developments that have allowed us to record simultaneously the first atomically resolved, real-space images of well-defined surface electronic quantum states of Si(111)-(7×7) and Si(001)-(2×1) surfaces, together with images at particular bias voltages that reflect the surface geometric structure (6). These sets of images reveal the close connection between surface geometry and surface electronic structure and allow us to assign the surface states long known from surface electron spectroscopies to specific features of the surface geometric structure. The new techniques discussed here allow spectroscopic studies to be performed on a surface area as small as  $4 \text{ \AA}^2$ , that is, on a single atom.

## Current Imaging Tunneling Spectroscopy (CITS)

In a scanning tunneling microscope (2), a fine tip is brought so close to the surface that the wave functions of the tip and the sample overlap. When a voltage is applied between tip and sample, electrons can tunnel through the vacuum barrier, and a tunneling current is established. The tip is mounted on three orthogonal piezoelectric transducers. As the tip is scanned along the surface, the tunneling current tends to increase (decrease) as the separation between sample and tip decreases (increases). In almost all experiments to date, however, the tunneling current is maintained at a constant value by a feedback circuit that applies a correction voltage to the  $z$  transducer normal to the surface. This correction voltage is measured as the tip is raster scanned along the surface and tracks the height fluctuations of the surface. It can be presented as a gray-scale image of the surface corrugations.

One such image obtained on the Si(111)-(7×7) surface is shown in Fig. 1. One (7×7) unit cell is outlined. Surface protrusions are white and depressions are black. The unit cell consists of two

The authors are at IBM Thomas J. Watson Research Center, Yorktown Heights, NY 10598.

equilateral triangles, and each triangle contains six distinct protrusions. At the corners of the unit cell, deep depressions are observed, referred to here as cornerholes. In addition, one half of the unit cell appears to be slightly higher than the other half. The image shown here is similar to the original result obtained by Binnig and co-workers (2), who interpreted the 12 maxima as being due to so-called adatoms. It has recently become clear (7) that in addition to these adatoms the  $(7 \times 7)$  surface contains structural elements that are not so easily discernible in Fig. 1.

At a given bias voltage, the magnitude of the tunneling current depends not only on the separation between tip and sample but also on the wave functions through which tunneling occurs. In Fig. 2, two schematic diagrams of the electronic energy levels in the tip region are shown. The tip was assumed to be a metal, the sample a semiconductor. In the semiconductor, the valence band is separated from the conduction band by a forbidden zone called the band gap, and the Fermi level ( $E_{FS}$ ) is inside the band gap. The valence band is completely filled, and the conduction band is empty. In the metal tip the states below the Fermi level ( $E_{FT}$ ) are filled; above  $E_{FT}$  they are empty. At the semiconductor surface, there are additional energy levels associated with the surface that extend into the bulk band gap.

In Fig. 2A, the sample is biased positive relative to the tip. Electrons flow from the filled states below the Fermi level of the tip into empty states above the Fermi level of the semiconductor. In Fig. 2B the sample is biased negative, and electrons flow from filled states below the Fermi level of the sample into empty states above the Fermi level of the tip. Only states between  $E_{FS}$  and  $E_{FT}$  contribute to the tunneling process. Thus by changing the applied bias voltage, the states that contribute to the tunneling current can be selected. The bias condition of Fig. 2A senses the empty states of the semiconductor, whereas in Fig. 2B the filled states of the semiconductor are probed. As the bias voltage between tip and sample is increased, the tunneling conductance increases each time the Fermi level of the tip passes through a new electronic state of the sample. Thus in measurements of the tunneling conductance ( $I/V$ ) as a function of voltage, surface states show up as a steplike increase in the conductance. The voltages at which such increases occur correspond with the energies of the surface state relative to the Fermi level of the semiconductor. By measuring such conductance-voltage curves in each pixel of an STM image while maintaining a constant separation between sample and tip, sufficient information can be obtained to generate real-space images of the surface electronic states.

There are various problems to overcome in this experiment. First, if there are no states between  $E_{FT}$  and  $E_{FS}$  there will be no tunneling, and the tip will be driven into the surface and frequently crash into the sample. On semiconductors this situation is quite common for biases within 0.5 V of  $E_{FS}$ . Second, because the feedback circuit keeps the tunneling current constant, the distance between tip and sample is not constant when the voltage is changed. In fact, the tip distance not only changes in response to the change in applied voltage but also as a result of a change in tunneling associated with the presence or absence of electron states at these energies. Finally, it appears to be impractical to measure complete conductance-voltage curves in each point of an STM image because of the time it would take to complete such a measurement and the microscope drifts occurring during the experiment.

We have circumvented these problems in the following way (6). Instead of monitoring the tunneling current continuously, the feedback electronics measures the tunneling current only 20% of the time—100  $\mu\text{sec}$  during each period of 500  $\mu\text{sec}$ —and updates the correction voltage applied to the  $z$  transducer accordingly. During the remaining 400  $\mu\text{sec}$ , the feedback circuit is inactive and the sample-tip separation is fixed. In these 400  $\mu\text{sec}$  the bias voltage and

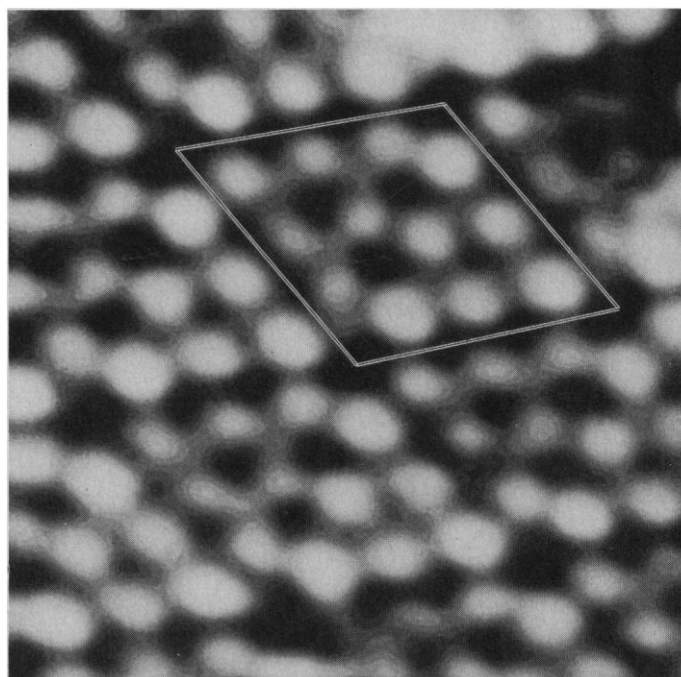


Fig. 1. STM image of Si(111)- $(7 \times 7)$  obtained with  $-2$  V applied to the sample. One  $(7 \times 7)$  unit cell has been outlined. The length of the short diagonal is 26.88  $\text{\AA}$ . The black-to-white range corresponds to a 2- $\text{\AA}$  displacement of the  $z$  transducer.

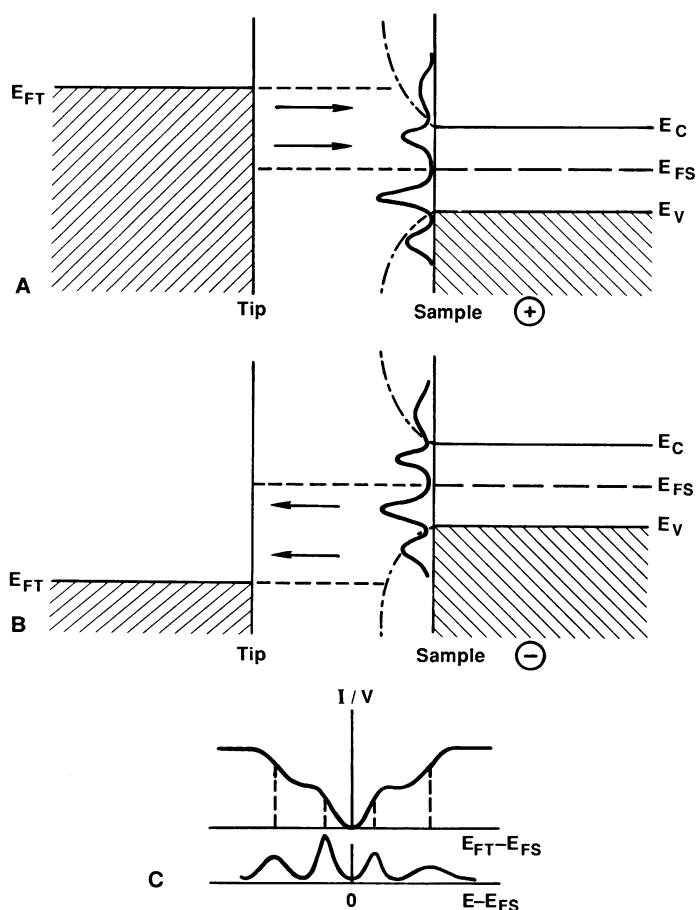


Fig. 2. Relative energy levels between tip and sample under positive (A) and negative (B) bias conditions. In (C) the relation between surface state energies and conductance onsets is shown. Symbols:  $E_{FS}$  and  $E_{FT}$ , Fermi levels of sample and tip;  $E_v$ , the top of the semiconductor valence band;  $E_c$ , the bottom of the conduction band;  $E$ , electron energy.

resulting tunneling current can be varied at will. A complete conductance-voltage curve can be measured by ramping the voltage over the desired range and measuring the tunneling current as a function of voltage with a number of parallel measuring channels. In our present setup, we can measure up to 48 points on a conductance-voltage curve together with the correction voltage applied to the  $z$  transducer in a  $150 \times 150$  pixel matrix. These roughly  $10^6$  measurements are performed in about 5 minutes. In each pixel of the topographic image, a complete conductance-voltage curve is obtained at constant sample-tip separation. In addition, it is possible to select a feedback bias voltage such that the tip closely follows the expected geometric corrugations of the atomic charge density of the surface (8). In this case the current (or conductance) images measured at voltages other than the feedback voltage largely reflect the surface electronic states without the contribution from the underlying geometric structure.

### Geometric Structure: Si(111)-(7×7)

As explained above, the corrugations recorded by the tip depend not only on the surface geometry but also on the surface electronic structure. Given a structural model one might hope to calculate the wave function overlap between tip and sample on the basis of a self-consistent scheme for solving Schrödinger's equation for this particular problem. Such a calculation is beyond the reach of present-day computers and electronic structure calculations, however, and a direct comparison of measured and calculated STM images will not be possible for many years to come. Nevertheless, for simpler cases than the (7×7) reconstruction much theoretical work has been done. Tersoff and Hamann (9) demonstrated that, for vanishingly small bias voltages applied between a metal (gold) sample and a tip with simple  $s$ -like wave functions, the corrugations measured by the STM closely correspond with surfaces of constant charge density. They also showed how under these conditions self-consistent calculations are closely approximated by superposition of atomic charge densities. Although the STM results we seek to analyze are different from theirs (large bias voltages and strong contributions from surface states), atomic charge superposition (ACS) calculations are of value in that they provide a well-defined reference image characteristic of the surface geometric structure only. In our calculations all atoms in the solid are treated as mutually independent, and surface states are explicitly not taken into account. Thus, although these calculations do not represent the real surface, they become useful later in delineating the surface states in our measurements.

Many different models have been proposed to explain the STM results of Binnig and co-workers (2). The number of broken bonds per unit cell in these models ranges from 19 to 97 (the ideal surface has 49 broken bonds in the same surface area) (10). Some of these models have adatoms; others invoke bond rearrangements giving rise to fivefold and sevenfold rings; still others propose adatom clusters instead of single adatoms (10). A number of models feature surface stacking faults in one or both halves of the unit cell, with dimers along the edges of the faulted regions. The wide variety of structural features present in all these models indicates both the complexity of the problem and the lack of knowledge and understanding of the physics of surface reconstruction. Because of the inability to compare these models directly with experimental STM images, the structure of this surface has remained controversial. We have used the ACS method to calculate STM images (surfaces of constant charge density) for many of these models, not only to test structural models but also to assess the usefulness of ACS calculations.

A comparison of images calculated for the models proposed by

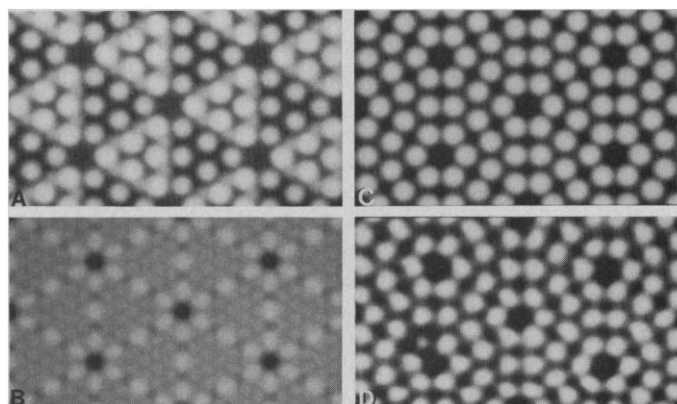


Fig. 3. STM images calculated for Chadi's model (A), McRae's model (B), and Takayanagi's model (C). An experimental image obtained with +2 V applied to the sample is shown in (D).

Chadi (12 adatoms and five- and sevenfold rings along the unit cell edges) (11), by McRae (surface stacking faults in both halves of the unit cell) (12), and by Takayanagi and co-workers (12 adatoms and a surface stacking fault in one half of the unit cell) (13) with the experimental result obtained with +2 V applied to the sample is shown in Fig. 3. The models by Chadi and McRae agree poorly with the data. (The agreement between Chadi's model and the image shown in Fig. 1 is somewhat better, but not much.) Other models also give poor agreement (8). Takayanagi's model, however, follows the experimental corrugations to within about 0.1 Å over the complete unit cell, with the exception of the cornerhole, where the deviation (as a result of limited experimental resolution) is somewhat larger. This striking agreement is a strong indication of the correctness of this model.

Figure 4 shows Takayanagi's model. The (7×7) unit cell is divided in two equilateral triangles. In the lower half of the cell, the crystal maintains the cubic diamond structure up to the last complete atomic layer. In the top half, however, the surface contains a

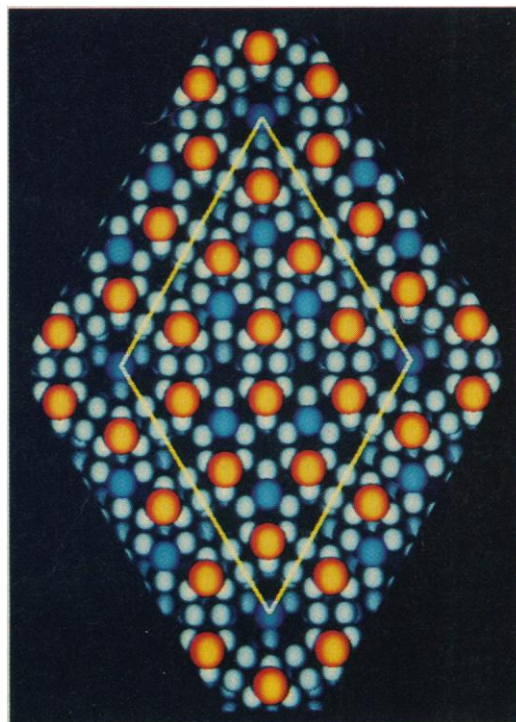


Fig. 4. Si(111)-(7×7) structure according to the model by Takayanagi (13).

stacking fault that is due to a rotation of the bond directions in the outer layer by  $60^\circ$ . The faulted and unfaulted regions of the unit cell are tied together by dimer bonds along the edges of the two triangles. On top of this structure, 12 additional atoms are adsorbed. These so-called adatoms bond to three atoms in the surface plane, consuming three dangling bonds and replacing these by a single dangling bond. Dangling bonds are present on the 12 adatoms (yellow-red), on 6 so-called restatoms in the underlying layer (light blue), and on 1 atom inside the hole at the corner of the unit cell (dark blue). Thus the number of dangling bonds in the  $(7 \times 7)$  cell is reduced from 49 to 19 by this complicated reconstruction. The reduction of dangling bonds is the driving force for the rearrangement of surface bonds; indeed, this model has the lowest number of broken bonds of all models that have been proposed for this surface.

The quantitative agreement between the calculations for Takayanagi's model and the experiments was somewhat of a surprise in view of the assumptions in the calculations. We have found, however, that similar agreement between theory and experiments can be obtained on the  $\text{Si}(001)-(2 \times 1)$  surface (14). Thus a comparison of ACS calculations with bias-dependent STM images may be used to evaluate structural models and to find bias conditions under which the recorded STM images closely reflect the geometric structure, without appreciable distortions by localized surface electronic states. In applying the ACS method it should be kept in mind that strongly localized surface states and the microscopic shape of the tip may appreciably affect the STM image.

## Electronic Structure: $\text{Si}(111)-(7 \times 7)$

At negative bias voltages, the STM images display a pronounced asymmetry between the two halves of the unit cell that cannot be explained by the surface geometric structure (Fig. 1). This asymmetry must be due to differences in surface electronic structure between the two halves of the unit cell. We have also shown that a bias condition can be selected in which the tip closely follows a charge density contour characteristic of the atomic structure of the surface. If this bias voltage is used to stabilize the separation between sample and tip, the CITS technique explained above will yield conductance data and current images that reveal the electronic structure of the surface. In Fig. 5A, conductance-voltage data obtained in selected  $4\text{-}\text{\AA}^2$  regions of the  $(7 \times 7)$  unit cell are shown. For comparison a solid line that represents the average conductance over one full unit cell is also shown. In the averaged data there are steplike increases in the conductance at 0.15, 0.8, and 1.7 V below  $E_{\text{FS}}$  and at 0.25 and 1.2 V above  $E_{\text{FS}}$ . These steplike increases signify the presence of surface states at these energies. These (small) increases in the average conductance are found to arise from strongly localized electronic states. For instance, the state at 0.8 V below  $E_{\text{FS}}$  gives rise to a fivefold increase in tunneling conductance between the three adatoms closest to the cornerholes in each side of the unit cell, whereas the occupied state just below  $E_{\text{FS}}$  is localized on the adatoms. For comparison, Fig. 5B shows results of ultraviolet photoemission spectroscopy and bremsstrahlung (isochromat) spectroscopy experiments (15). The surface states observed with these techniques show a one-to-one correspondence with the onsets in tunneling conductance that are expected to arise from tunneling through the surface states as described above.

These surface states can be selectively imaged by taking current images just below and above the observed onsets and subtracting them on a computer. This difference image yields a direct two-dimensional representation of the surface state giving rise to the selected onset. Figure 6A shows an image of the most weakly bound surface electrons, which are just below  $E_{\text{FS}}$ . These quantum states

are localized on the adatoms and display a marked asymmetry between the two halves of the unit cell. In addition, the states closest to the cornerholes appear stronger than those closest to the center of each half of the unit cell. The surface state at 0.8 V below  $E_{\text{FS}}$  is imaged in Fig. 6B. This state is localized on the six restatoms in the layer beneath the adatoms and on the broken bond inside the cornerhole. In Fig. 6, A and B, we see all the dangling bond states of the  $\text{Si}(111)-(7 \times 7)$  surface, 19 per unit cell. The mirror symmetry of the broken-bond states on the restatoms with respect to the short diagonal of the unit cell indicates a mirror symmetry of the atomic positions in the two halves of the unit cell. This directly proves the presence of a stacking fault in one half of the unit cell. Thus both the number of dangling bonds and their geometric location are in excellent agreement with Takayanagi's model.

The state at 1.7 V below  $E_{\text{FS}}$  is imaged in Fig. 6C. It is localized between the adatoms and appears to be associated with the back bonds between the adatoms and the underlying crystal. Thus, although sources other than surface states may contribute to these images (for instance, position and voltage dependence of the tunneling barrier), it is clear that from these results the surface states long known from photoemission can be directly identified with specific atomic features in the surface structure. This identification has gained additional support from the recent theoretical work by Northrup (16), who found the same surface states in calculations performed for  $(\sqrt{3} \times \sqrt{3})$  and  $(2 \times 2)$  subunits of the  $(7 \times 7)$  unit cell.

The states on the restatoms are 0.8 eV below  $E_{\text{FS}}$  and must therefore be completely occupied. Thus these broken-bond orbitals have a lone-pair character. In his calculations on a  $(2 \times 2)$  unit cell

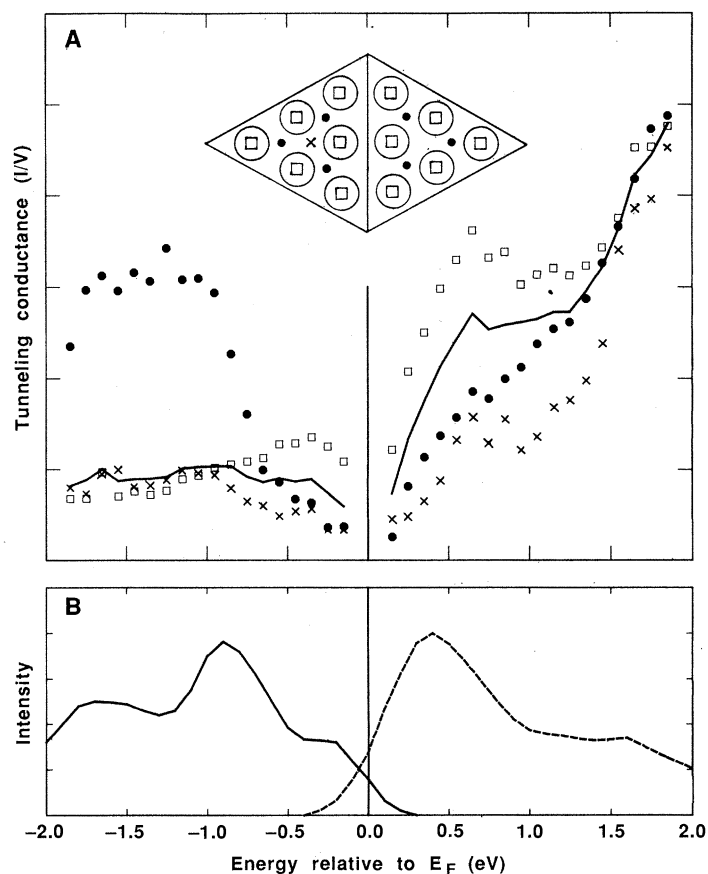


Fig. 5. (A)  $I/V$  curves for selected points in the  $(7 \times 7)$  unit cell (symbols) and averaged over one unit cell (solid line). (B) Filled and empty surface states observed with ultraviolet photoemission and bremsstrahlung spectroscopies [after (15)].  $E_{\text{F}}$ , Fermi level.

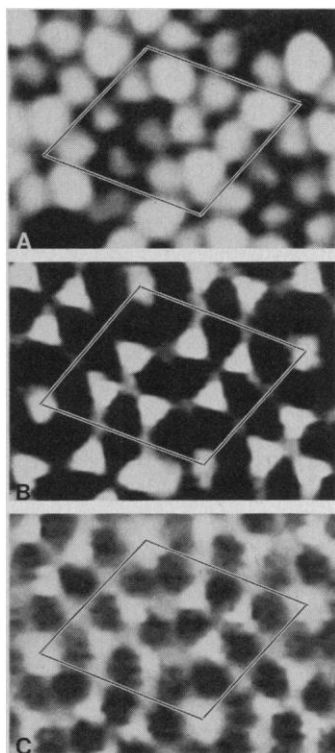


Fig. 6. Filled surface states on the Si(111)-(7×7) surface. (A) Adatom state at -0.35 V. (B) Dangling bond state at -0.8 V. (C) Back bond state at -1.7 V.

containing one adatom and one restatom, Northrup found that the restatom state is completely filled and that the adatom state is empty (16). In a simple picture, one electron has gone from the adatom to the restatom. In each half of the unit cell the central three adatoms each have two restatom neighbors, whereas the adatoms closest to the cornerholes have only one restatom neighbor. Therefore the central three adatoms “lose” more of their charge to the restatoms than the three corner adatoms. Because the ratio of restatoms to adatoms is less than 1, none of the adatom dangling bond orbitals gives up all its charge, and this surface state is located just below  $E_{FS}$ . Also, an empty surface state on the adatoms is directly above  $E_{FS}$ . This is consistent with one adatom-derived surface state straddling  $E_{FS}$ . In the faulted half of the unit cell the surface state on the restatoms is 0.1 eV closer to  $E_{FS}$  than in the unfaulted half, and the maximum tunneling current into these states is smaller in the faulted half than in the unfaulted half. This indicates that, although similar, the restatom states are not the same in the two halves of the unit cell. In particular, the density of states in the faulted half appears to be smaller than in the unfaulted half. Hence the amount of charge transferred from adatom to restatom is smaller in the faulted half, and the density of states on the adatoms is larger. This gives rise to the asymmetry in Fig. 6A and Fig. 1. The difference in electronic structure between the two halves of the unit cell is not surprising. In fact, the restatoms themselves are part of the layer that constitutes the stacking fault, and their electronic structure should bear this signature.

### Geometric and Electronic Structure: Si(001)-(2×1)

The Si(001) surface has a different termination than the Si(111) surface because the surface cuts the bulk crystallographic unit cell along a different direction. Again, many different structural models have been proposed for this surface. In a recent STM study we showed that pairs of surface atoms initially separated by 3.84 Å decrease their interatomic distance to form a bond and thus decrease

the number of broken bonds in the surface by a factor of 2 (14). These unusual pairs of surface atoms are called dimers.

In Fig. 7 we show both filled (A) and empty (B) surface states obtained on the Si(001)-(2×1) surface. The image in Fig. 7A is a conventional STM image obtained with -2 V applied to the sample. The gray-scale range is 1 Å. Between 0 and -2 V, the current images are featureless because there is only one occupied surface state associated with the dimer bond. Therefore, this “topographic” image is also the image of the occupied surface states. We have also shown (14) that under these feedback bias conditions the tip follows closely the geometric corrugations as derived from ACS calculations for dimer models.

In Fig. 7A the dimer structure of the surface gives rise to the rows of oblong protrusions. The rows are 7.68 Å apart; the dimers in the rows are only 3.84 Å apart. The bonding states are located on the centers of the dimers in most of the image. The zig-zag patterns in the upper right-hand corner primarily occur close to defects. They

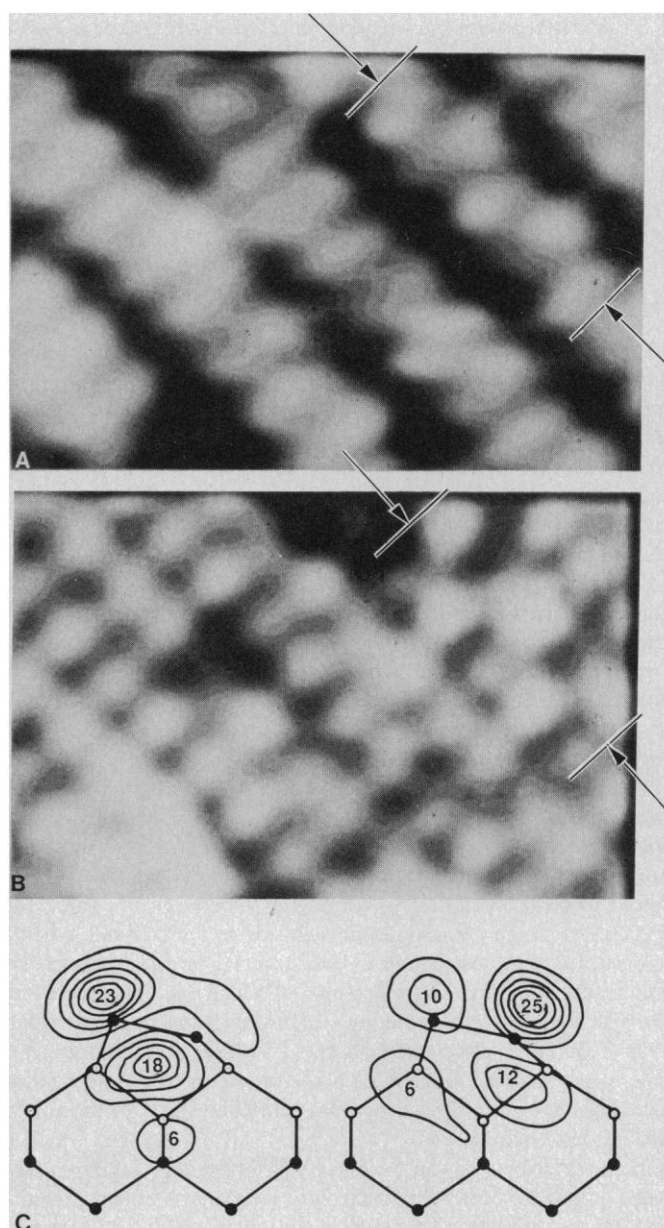


Fig. 7. Filled (A) and empty (B) surface states on the Si(001)-(2×1) surface. Theoretical charge density contours of the filled and empty surface states on a buckled dimer are shown in (C) [after (17)].

are easily attributed to buckling of the dimers. Alternate dimers along the row buckle in opposite directions, tilting the dimer bond axis out of the plane.

Figure 7B was obtained with +2 V applied to the sample and was recorded simultaneously with Fig. 7A. On the symmetric dimers (lower left in Fig. 7, A and B), empty states are found at both ends of the dimers, as expected. On the buckled dimers the empty states are strongest on the lowered side of the dimer, that is, on the side where the occupied surface state is weakest. This can be seen from the fact that the zig-zag in the empty states is out of phase with the zig-zag in the occupied states.

Figure 7C shows a theoretical contour plot of the self-consistent charge density in the occupied surface state (left) and the unoccupied surface state (right) on a buckled dimer (17). The spatial nature of these surface states, as predicted by this quantum mechanical calculation (17), is in striking agreement with the experimental result. There is also a gap between the occupied and unoccupied surface states, in good agreement with results of ultraviolet photoemission and bremsstrahlung spectroscopic studies. Atomic-scale defects and structural irregularities often give rise to electronic states inside this surface-state band gap.

## Future Directions

The scanning tunneling microscope can be used to study both atomic and electronic structure of surfaces with a lateral resolution of 2 to 3 Å. The CITS technique has already revealed the direct correlation between surface geometric structure and quantum states on Si(111)-(7×7) and Si(001)-(2×1) surfaces. On the (7×7) surface, the surface states long known from conventional techniques can now be assigned to specific features of the surface atomic structure. Even the number of dangling bonds per unit cell can be directly counted: 19 instead of the 49 broken bonds in the bulklike terminated surface. On the (2×1) surface, the basic structural unit (dimer) and the bonding and antibonding states in these dimers have been observed, providing a direct illustration of simple molecular orbital theory.

With this new understanding, every STM experiment is an exercise in surface spectroscopy: the quantum states at the surface dominate what is observed. From the examples discussed it becomes clear that this presents a marvelous opportunity to study the surface electronic structure, atom by atom. The study of atom-size defects

(with low density) is one of the most obvious avenues. Such defect states are of crucial importance in electronic devices. Schottky barriers are believed to be strongly determined by defects formed in semiconductor surfaces by submonolayers of metal films (18). The electronic structure of such defects can now be determined directly.

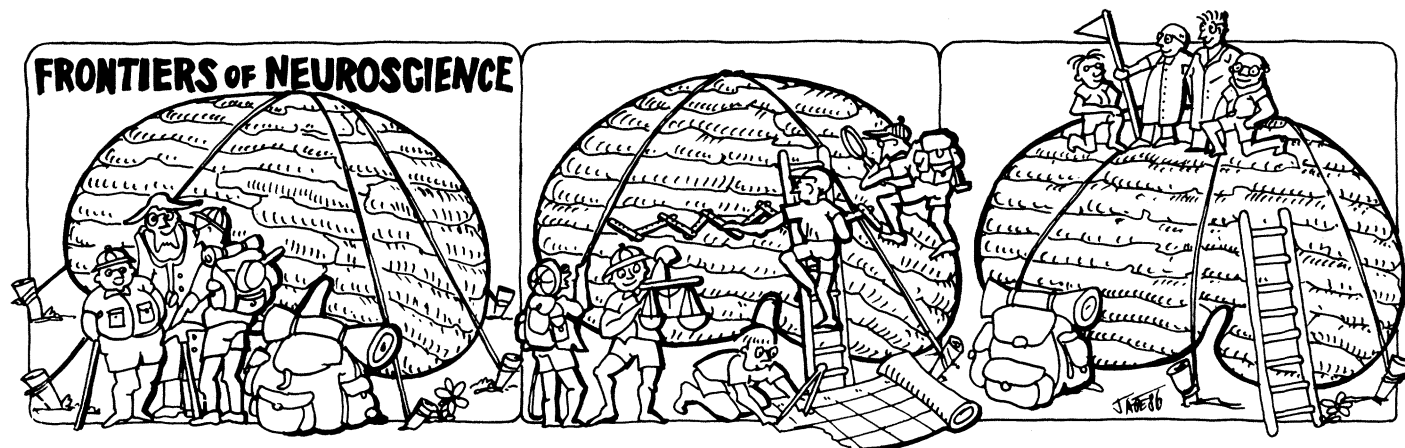
Surface chemistry presents itself as another exciting field of investigation. Electronic states can be used as labels by which to recognize different atoms and molecules on surfaces. Surface states localized at defects such as steps and kinks may be identified, and the changes in these states upon adsorption of foreign elements may give important clues about their role in both poisoning and promotion of catalysis.

In thin oxides, electronic states have already been observed (19) in which an electron may be trapped for milliseconds. Such trap states are important for the electrical integrity of oxide films on semiconductors. Further atomically resolved studies of such states will lead to a better understanding of their correlation with atomic geometry.

Most important, the scanning tunneling microscope has now bridged the gap between surface electronic structure and surface geometric structure and has fulfilled the theorist's dream (or nightmare) in which calculation and experiment can be compared on an atomic level.

## REFERENCES AND NOTES

1. For a survey of the many techniques to study surfaces, see M. A. van Hove and S. Y. Tong, Eds., *The Structure of Surfaces* (Springer-Verlag, Berlin, 1985).
2. G. Binnig, H. Rohrer, C. Gerber, E. Weibel, *Phys. Rev. Lett.* **50**, 120 (1983).
3. J. J. Lander and J. Morrison, *J. Appl. Phys.* **34**, 1403 (1963).
4. J. A. Golovchenko, *Science* **232**, 48 (1986).
5. R. M. Feenstra, W. A. Thompson, A. P. Fein, *Phys. Rev. Lett.* **56**, 608 (1986).
6. R. J. Hamers, R. M. Tromp, J. E. Demuth, *ibid.*, p. 1972.
7. A. L. Robinson, *Science* **232**, 451 (1986).
8. R. M. Tromp, R. J. Hamers, J. E. Demuth, *Phys. Rev. B* **34**, 1388 (1986).
9. J. Tersoff and D. R. Hamann, *ibid.* **31**, 805 (1985).
10. R. M. Tromp and E. J. van Loenen, *Surf. Sci.* **155**, 441 (1985).
11. D. J. Chadi, *Phys. Rev. B* **30**, 4470 (1984).
12. E. G. McRae, *Surf. Sci.* **124**, 106 (1983).
13. K. Takayanagi, T. Tanishiro, M. Takahashi, S. Takahashi, *J. Vac. Sci. Technol.* **A3**, 1502 (1985).
14. R. M. Tromp, R. J. Hamers, J. E. Demuth, *Phys. Rev. Lett.* **55**, 1303 (1985); unpublished results.
15. F. J. Himpsel and T. Fauster, *J. Vac. Sci. Technol.* **A2**, 815 (1984).
16. J. E. Northrup, *Phys. Rev. Lett.* **57**, 154 (1986).
17. J. Ihm, M. L. Cohen, D. J. Chadi, *Phys. Rev. B* **21**, 4592 (1980).
18. L. J. Brillson, *Surf. Sci. Rep.* **2**, 123 (1982).
19. M. E. Welland and R. H. Koch, *Appl. Phys. Lett.* **48**, 724 (1986).
20. We thank P. Schroer and J. Becker for their assistance in setting up the electronics and the data acquisition programs; M. Welland for contributions during the initial construction of the microscope; and J. Tersoff and N. Lang for stimulating discussions.



At The **AAAS** Annual Meeting, 14-18 February 1987, in Chicago  
(See 12 December issue of *SCIENCE* for details)